Resonant x-ray scattering reveals possible disappearance of magnetic order under hydrostatic pressure in the Kitaev candidate γ-Li$_2$IrO$_3$

Nicholas P. Breznay,[1,2,*] Alejandro Ruiz,[1,2] Alex Frano,[1,3] Wenli Bi,[4,5] Robert J. Birgeneau,[1]
Daniel Haskel,[4] and James G. Analytis[1,2]

[1]*Department of Physics, University of California, Berkeley, Berkeley, California 94720, USA*
[2]*Materials Science Division, Lawrence Berkeley National Laboratory, Berkeley, California 94720, USA*
[3]*Advanced Light Source, Lawrence Berkeley National Laboratory, Berkeley, California 94720, USA*
[4]*Advanced Photon Source, Argonne National Laboratory, Argonne, Illinois 60439, USA*
[5]*Department of Geology, University of Illinois at Urbana-Champaign, Urbana, Illinois 61801, USA*

Honeycomb iridates such as γ-Li$_2$IrO$_3$ are argued to realize Kitaev spin-anisotropic magnetic exchange, along with Heisenberg and possibly other couplings. While systems with pure Kitaev interactions are candidates to realize a quantum spin-liquid ground state, in γ-Li$_2$IrO$_3$ it has been shown that the presence of competing magnetic interactions leads to an incommensurate spiral spin order at ambient pressure below 38 K. We study the pressure sensitivity of this magnetically ordered state in single crystals of γ-Li$_2$IrO$_3$ using resonant x-ray scattering (RXS) under applied hydrostatic pressures of up to 3 GPa. RXS is a direct probe of electronic order, and we observe the abrupt disappearance of the $\mathbf{q}_{\rm sp} = (0.57, 0, 0)$ spiral order at a critical pressure $P_c = 1.4$ GPa with no accompanying change in the symmetry of the lattice.

Honeycomb magnetic materials with strong spin-orbit coupling were recently proposed to realize spin-anisotropic "Kitaev" magnetic exchange [1] and therefore to host a highly entangled spin-liquid ground state with fractionalized excitations [2,3]. Additional interactions (such as Heisenberg or next-nearest-neighbor couplings) that compete with the Kitaev exchange can stabilize many possible spin orders [4–8]. For example, the layered compounds Na$_2$IrO$_3$ and RuCl$_3$, composed of edge-sharing IrO$_6$ or RuCl$_6$ octahedra, show a zigzag spin texture [9–11]. The three-dimensional (3D) harmonic honeycomb β and γ polytypes of Li$_2$IrO$_3$ [12,13] both exhibit an incommensurate spiral order [14,15]. These magnetic ground states derive from the balance of Kitaev (K), Heisenberg (J), and other possible couplings between spins $\vec{S}_i$ in the Hamiltonian

$$H = \sum_{\substack{i,j \\ \gamma \in x,y,z}} \left(K S_i^\gamma S_j^\gamma + J \vec{S}_i \cdot \vec{S}_j + \cdots \right). \tag{1}$$

Here the $\gamma = x,y,z$ Kitaev exchange directions couple spins that are perpendicular to the planes formed by adjacent edge-sharing IrO$_6$ octahedra, shown for γ-Li$_2$IrO$_3$ in Figs. 1(a) and 1(b).

With such a delicately balanced Hamiltonian, minor changes in its parameters may result in a drastic alteration of the magnetic ground state. These changes may tune away from long-range magnetic order and perhaps towards unexplored phases such as a quantum spin liquid. One experimental approach to achieving this goal is to apply an external perturbation and study the evolution of the magnetic ground state. For example, a magnetic field applied to β-Li$_2$IrO$_3$ suppresses the spiral order and stabilizes a canted zigzag spin texture, as observed by recent resonant x-ray scattering studies [16].

Hydrostatic pressure can also be a useful control parameter. X-ray magnetic circular dichroism (XMCD) experiments on β-Li$_2$IrO$_3$ suggest the disappearance of the material's ferromagnetic response in $\mu_0 H = 4$ T near 2 GPa, which has been put forth as evidence of a new magnetic ground state [13]. However, the lack of momentum space (Q) resolution of XMCD leaves open the question of which of the nearby magnetic phases responds to hydrostatic pressure. High-pressure setups pose broad experimental challenges for techniques (such as magnetic x-ray scattering) that track individual magnetic orders; to date there have been no such studies under pressure in the honeycomb iridates.

Recent developments in high-brightness synchrotron x-ray sources have allowed for a high-pressure apparatus to be integrated in a resonant x-ray scattering (RXS) experiment. RXS directly probes electronic and magnetic orders resolved in Q space by tuning the energy of incident x rays to be on resonance with an element's absorption edge. The resulting scattering process is sensitive to both charge and magnetic order of the valence electrons. At the Ir $L_{2,3}$ edge, for example, the intermediate states in the scattering process are sensitive to both the spin and orbital character of the $5d$ hole states [17]. RXS is particularly useful when neutron scattering is rendered unfeasible by small sample sizes or elements with large neutron absorption cross sections like iridium. Thus, the enhanced cross section at the Ir L_3 resonance along with the large Ewald sphere afforded by 11.215 keV x rays has made RXS the best-suited scattering technique to investigate the ambient-pressure magnetic order in the honeycomb iridates γ-Li$_2$IrO$_3$ [15], β-Li$_2$IrO$_3$ [14], and Na$_2$IrO$_3$ [18]. RXS studies under applied pressure, however, are strongly constrained by the apparatus geometry and resulting limitations on the sample dimensions and available reciprocal space. As a result, the precise influence of hydrostatic pressure on the ground state of Kitaev honeycomb iridates remains unknown.

In this work we use RXS to track the evolution of the γ-Li$_2$IrO$_3$ incommensurate spiral order with applied
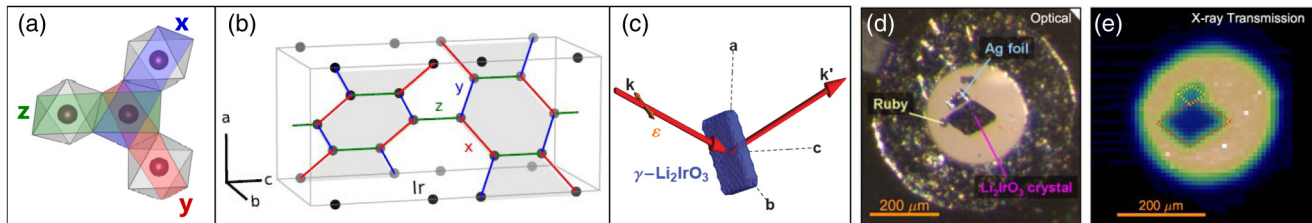
---

*nbreznay@berkeley.edu

FIG. 1. (a) Local geometry of edge-sharing IrO_6 octahedra and (b) 3D network of Ir atoms composed of intersecting honeycomb layers (gray) in the orthorhombic crystal structure of γ-Li_2IrO_3; x, y, z Kitaev bonds are highlighted in both panels. (c) Laue (transmission) scattering geometry; x rays with initial wave vector **k** and polarization ϵ scatter into **k′** within the Li_2IrO_3 crystallographic a-c plane. (d) Micrograph of the loaded diamond-anvil cell with a polished single crystal and Ag foil and ruby spheres for pressure calibration and *in situ* monitoring. (e) X-ray transmission image of the sample *in situ*; both γ-Li_2IrO_3 crystal and Ag foil are outlined.

hydrostatic pressure and observe the suppression of this magnetic phase. While we find no discontinuity in the lattice structure or an associated change in symmetry to the highest pressures measured, we observe an abrupt disappearance of the spiral Bragg peak at a critical pressure $P_c = 1.4$ GPa. This disappearance signals the transition to a distinct electronic ground state.

We begin by reviewing the details of our experimental procedure before presenting the experimental results and analysis. Single crystals of γ-Li_2IrO_3 were grown as described previously [12,16]. Figure 1(b) shows the intersecting Ir honeycomb layers in one unit cell of the orthorhombic *Cccm* crystal structure. To track the evolution of the spiral magnetic order in γ-Li_2IrO_3, RXS experiments were conducted using single crystals in a transmission (Laue) scattering geometry. Polished samples were 20–30 μm thick, chosen to match the absorption length of x rays near the Ir $L_{2,3}$ edges of $\sim$10 μm. The transmission scattering scheme is shown in Fig. 1(c). Samples were prealigned for scattering within the crystal a-c plane in a vertical geometry. The specular (H 0 0) direction was verified with several peaks, as described below. The polarization of the incoming x rays was horizontal (σ), with no polarization analysis of the scattered (π) beam. The magnetic scattering intensity, proportional [17] to $|\sum_i e^{i\mathbf{Q}\cdot\mathbf{r}_i}(\sigma \times \pi_{out}) \cdot \mathbf{m}_i|^2$, where $\mathbf{m}_i$ is the magnetic moment at site r_i, projects the component of $\mathbf{m}_i$ parallel to the outgoing wavevector **k′** (in the a-c scattering plane).

X-ray scattering studies under pressure (up to 3 GPa) and at temperatures between 5 and 300 K were performed at beamline 4-ID-D of the Advanced Photon Source at Argonne National Laboratory. Merrill-Bassett-type diamond-anvil cells (DACs) with 800-μm culets were used with stainless-steel gaskets of 250 (150) μm initial (preindented) thicknesses, with 400-μm sample chamber holes [19]. The gaskets were loaded with γ-Li_2IrO_3 single crystals (cross-sectional area 150$\times$100 μm^2), along with several ruby balls and 40$\times$40 μm^2 pieces of 12-μm-thick Ag foil for ambient- and low-temperature pressure calibration [20]. The pressure medium was a 4:1 methanol:ethanol mixture. After preparing the DAC, the cell pressure at ambient temperature was monitored using a custom-built optical spectrometer and a Raman system to measure the ruby $R1$ fluorescence peak. The target pressure on loading was $\sim$0.1 GPa. The pressure at low temperature was determined *in situ* using Ag powder peaks and

the isothermal bulk modulus of Ag at 5 K ($K_{Ag} = 110.85$ GPa, $K'_{Ag} = 6.0$ GPa) [20]. We estimate a systematic uncertainty of $\pm$0.1 GPa in the pressures quoted below by comparing the estimated pressure from (1 1 1), (2 0 0), and (2 2 0) Ag powder peaks and from repeated pressure measurements before and after scans.

All measurements reported were performed on two samples at the cryostat base temperature of 4.7 ± 0.5 K. Pressure was changed *in situ* using a helium membrane. Cell layout and sample status were checked after loading [see optical image in Fig. 1(d), showing diamond-shaped γ-Li_2IrO_3 crystal, Ag foil, and ruby spheres in the DAC gasket hole] and monitored using x-ray transmission maps [Fig. 1(e), obtained using a slit-defined 30$\times$30 μm^2 beam]. To track the absolute magnetic Bragg peak intensities with pressure, peak areas were normalized to the integrated (4 0 0) rocking curve intensities. The mosaic FWHM values are 0.05°–0.10° for sample 1 between 0 and 3 GPa and 0.01° for sample 2 at 2.0 GPa.

Based on the restricted scattering geometry imposed by the DAC, we focused our study on (H 0 0) peaks in reciprocal space. In γ-Li_2IrO_3, selection rules forbid the (1 0 0) and (3 0 0) lattice peaks, while the structure factor for the (2 0 0) order is strongly suppressed. Figure 2(a) shows a reciprocal space map of the (H 0 0) axis, where an intense structural (4 0 0) Bragg peak and weaker (2 0 0) peak are both observed. [In the β-Li_2IrO_3 polytype the (2 0 0) peak is forbidden.] Nonstructural peaks located at (4 $\pm$ 0.57 0 0) correspond to the incommensurate spiral magnetic order [14,15], which at ambient pressure appears below $T_{sp} = 38$ K. The main finding of this work is the disappearance of this peak at $P_c = 1.4$ GPa, shown in Fig. 2(b) at 4.7 K. The electronic nature of these peaks is confirmed by fixed-Q energy scans [Fig. 2(c)] showing a strong enhancement of the diffracted intensity near the 11.215 keV Ir L_3 resonance, in contrast to the weak background observed away from the spiral order peak at (4.42 0 0) that shows an increase of $\sim$10% above the Ir edge due to fluorescence.

Under applied hydrostatic pressure we observe a continuous reduction in the unit-cell volume with a large bulk modulus typical of iridates. Figure 3(a) shows the pressure dependence of the (4 0 0) Bragg peak (normalized), and the spiral order peak is shown in Fig. 3(b). The curves are vertically offset for clarity and labeled with the corresponding pressure; because of the fine incremental changes we quote the most
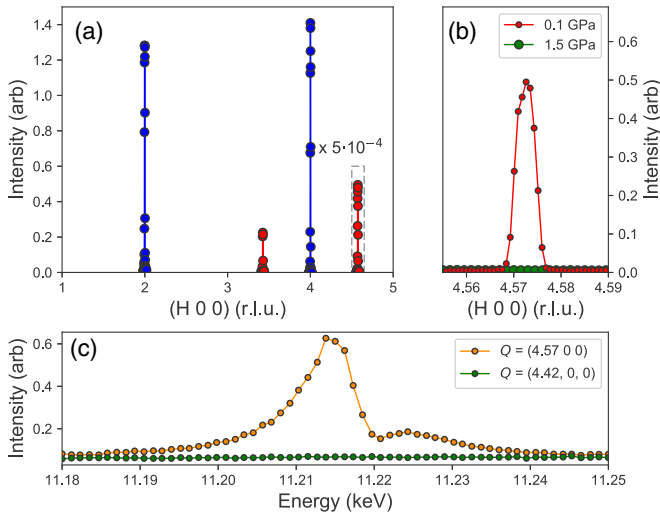
FIG. 2. (a) Magnetic (red) and structural (blue) Bragg peaks along the $(H\,0\,0)$ direction measured at 4.7 K; the $(4\,0\,0)$ peak has been scaled by a factor of 5×10^{-4}. (b) Close-up of the dashed region in (a) showing scans near $(4\,0\,0)+\mathbf{q}_{sp}=(4.57\,0\,0)$. The magnetic Bragg peak visible at 0.1 GPa (red) disappears abruptly above 1.4 GPa (green). (c) Energy scans at fixed $\mathbf{Q}=(4.57\,0\,0)$ and away from the magnetic peak $\mathbf{Q}=(4.42\,0\,0)$ showing a featureless background.
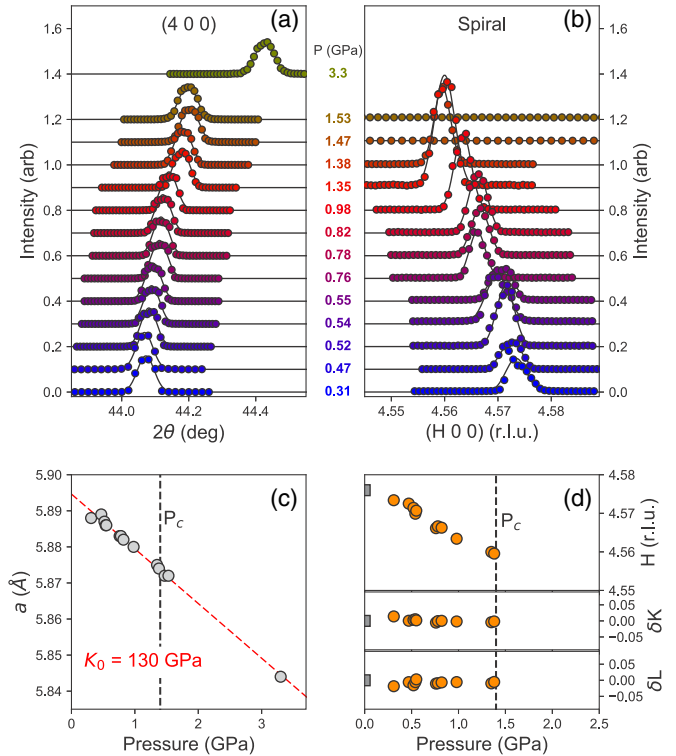

FIG. 3. Evolution under applied pressures from 0.3 to 3 GPa, as labeled, for (a) the $(4\,0\,0)$ Bragg peak intensity versus 2θ and (b) the spiral order peak. Solid lines are guides to the eye. (c) Decrease in lattice constant a with applied hydrostatic pressure, extracted from the $(4\,0\,0)$ structural Bragg peak; assuming a relative change in volume that is isotropic, the bulk modulus $K_0=130$ GPa. (d) Top: Decrease in the spiral order wave vector $\mathbf{q}_{sp}$ with applied pressure. The wave vector is not close to a commensurate value at P_c. Bottom: dependence of the magnetic peak's component along $(0\,K\,0)$ and $(0\,0\,L)$, relative to the position of the $(4\,0\,0)$ Bragg reflection. The gray squares were obtained from companion experiments at ambient pressure.

precise estimate for each pressure, suppressing the ±0.1 GPa systematic uncertainty. The shift in the 3.3 GPa $(4\,0\,0)$ scan is a consequence of a large pressure increment; the a-axis lattice parameter evolves linearly with pressure over the entire range studied, shown in Fig. 3(c). Also shown in Fig. 3(c) is a linear fit yielding $da/dP=-0.015$ Å/GPa. Assuming an isotropic fractional change in the unit-cell dimensions, the $T=4.7$ K bulk modulus $K_0=-\frac{1}{3}a(\frac{da}{dP})^{-1}=130\pm20$ GPa. Electronic structure calculations for β-Li$_2$IrO$_3$ indicate anisotropic compressibility of lattice parameters [21]. Recent diffraction experiments [22] report anisotropic compression and $K_0=100(8)$ GPa, significantly lower than 150-250 GPa values typical of other iridates [23,24].

Neither the $(4\,0\,0)$ Bragg peak amplitude nor width changes appreciably with increasing pressure, indicating that the crystal quality remains constant. Aside from contraction of the unit cell [shown in Fig. 3(c)], no structural changes were observed; the symmetry of the lattice appears intact throughout this pressure range.

Figure 3(b) shows the pressure evolution of the spiral order peak, tracking its position along the $(H\,0\,0)$ axis as the pressure increases. The incommensurate wave vector $\mathbf{q}_{sp}$, normalized to the change in lattice constant, decreases with increasing pressure, as shown in Fig. 3(d) (top panel); $\mathbf{q}_{sp}$ decreases by 0.3% before the spiral order disappears at P_c. The linear and continuous decrease observed in $\mathbf{q}_{sp}$, ending at an apparently irrational fraction, precludes an incommensurate-to-commensurate transition. Furthermore, we monitored the peak position along directions orthogonal to $(H\,0\,0)$ by performing angular motions (θ and χ scans). The magnetic peak position does not shift with respect to the Bragg reflection $(4\,0\,0)$ over the corresponding reciprocal space ranges shown in Fig. 3(d) (bottom panels). As the peak width is also

pressure independent, we conclude that $\mathbf{q}_{sp}$ is not continuously developing a component along K or L. Above an applied pressure of $P_c=1.4$ GPa, the spiral order peak is abruptly extinguished, as shown in Fig. 3(b). We scanned the entire accessible range of $2<H<6$ reciprocal lattice units as well as within the orthogonal ranges of Fig. 3(d) (bottom panels) and found no evidence for the incommensurate peaks anywhere in this reciprocal space volume.

To further consider the evolution of the spiral magnetic order, we integrate the $\mathbf{q}_{sp}$ peak intensity as a function of applied pressure, as shown in Fig. 4(a). To within the uncertainty associated with consistent realignment of the sample after changing pressure, the peak intensities gradually increase with pressure until abruptly disappearing at P_c. The otherwise identical sample 2 also showed no sign of the spiral order at 2.0 GPa, the only pressure studied. (The apparatus allows the pressure to be *increased* only after loading and cooling. For this sample, this initial pressure was 2.0 GPa.)

We present a schematic pressure-temperature phase diagram for γ-Li$_2$IrO$_3$ in Fig. 4(b); the dark region indicates
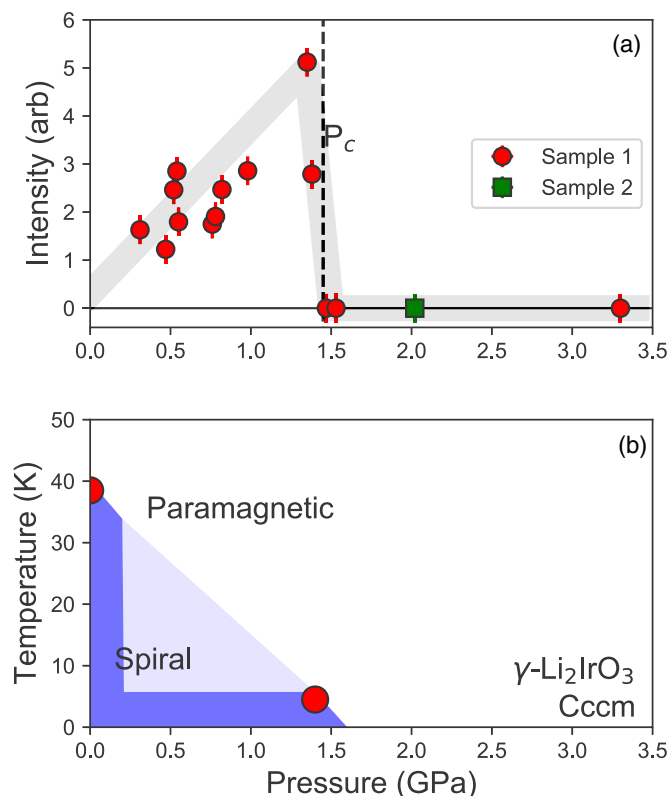
FIG. 4. (a) Magnetic Bragg peak intensity versus applied pressure for two samples. The intensity for sample 1 disappears abruptly at $P_c = 1.4$ GPa; no magnetic peak is observed at 2.0 GPa for sample 2. (b) Schematic pressure-temperature magnetic phase diagram for γ-Li$_2$IrO$_3$; the dark region indicates the extent of direct studies of the spiral-order phase to date. No discontinuous change in the lattice (space group *Cccm*) is observed to 3 GPa.

the observed extent of the spiral magnetic order, and the light shaded region represents the simplest associated phase boundary. Ongoing studies of this material indicate paramagnetic behavior with rapidly emerging magnetic anisotropy favoring the *b* (easy) axis direction [12,25] at ambient pressure. As *T* approaches 0 K, P_c likely continues to represent a sharp phase boundary between the spiral magnetic order and the as-yet undetermined high-pressure electronic phase; the sharp disappearance could signal a first-order quantum phase transition. As there is no change in the lattice symmetry and no symmetry-breaking field being used to perturb the material, it is unclear what ordered state may exist beyond P_c, if any.

Under an applied magnetic field, a correlated paramagnet which admixes the broken symmetry of zigzag order [16,26] appears to be the next competitive magnetic ground state at ambient pressure. However, the transition observed under applied magnetic field appears to be continuous, in contrast to the pressure-tuned transition at P_c; a different ground state may emerge in this case.

The effect of pressure on the crystal structure and associated Kitaev, Heisenberg, and other exchange couplings

was recently studied theoretically for β-Li$_2$IrO$_3$ [21]. In this closely related polytype, the Kitaev exchange coupling was predicted to decrease with increasing pressure above ambient conditions, disappearing at 5–10 GPa. If a similar evolution of the magnetic interactions appears in γ-Li$_2$IrO$_3$, our results firmly demonstrate that the spiral magnetic order is stabilized by Kitaev exchange and is suppressed as this mechanism weakens. This could also answer why the intensity of the spiral order peak grows with pressure. For example, relieving the Kitaev frustration may allow a greater share of the $J_{\text{eff}} = 1/2$ moment to appear in the incommensurate order before this state is suppressed at P_c. Finally, experimental studies of pressure evolution of the local Ir environment in Li$_2$IrO$_3$ will also allow for a quantitative analysis of how the change in structure serves to push this material closer to or farther from the pure Kitaev limit.

The scale of P_c is modest compared to the 17 GPa required to suppress weak ferromagnetism in Sr$_2$IrO$_4$ [27]. The pressure roughly corresponds to an energy density of 9 meV/Å^3, or 0.08 eV/Ir; while less than both the spin-orbital energy $\lambda_{\text{SO}} \sim$ 0.2–0.5 eV and electronic interaction $U \sim 0.5$ eV that have been reported in 5*d* iridate materials [27–29], it is beyond the ~ 1 meV scale that was proposed to separate β-Li$_2$IrO$_3$ from a 3D spin-liquid state [30]. Mixing of the (nominally filled) $J_{\text{eff}} = 3/2$ manifold of states could serve to disrupt the $J_{\text{eff}} = 1/2$ doublet that stabilizes the unconventional magnetic orders in these materials. Such a picture could be investigated quantitatively with high-pressure studies of x-ray absorption and XMCD spectroscopies that provide a quantitative probe of the spin and orbital components of the local magnetic moments.

In summary, we are able to observe the disappearance of the spiral magnetic order in γ-Li$_2$IrO$_3$ at an applied pressure of 1.4 GPa by conducting resonant x-ray scattering studies at the Ir L_3 edge. This observation provides strong evidence for tunability of the Kitaev, Heisenberg, and other magnetic exchange couplings with applied pressure. Future resonant diffraction studies will be able to incisively address the possibility of complete disappearance of long-range magnetic order in the high-pressure ground state of this Kitaev candidate material.

[1] G. Jackeli and G. Khaliullin, Mott Insulators in the Strong Spin-Orbit Coupling Limit: From Heisenberg to a Quantum Compass and Kitaev Models, Phys. Rev. Lett. **102**, 017205 (2009).

[2] A. Kitaev, Anyons in an exactly solved model and beyond, Ann. Phys. (NY) **321**, 2 (2006).

[3] W. Witczak-Krempa, G. Chen, Y. B. Kim, and L. Balents, Correlated quantum phenomena in the strong spin-orbit regime, Annu. Rev. Condens. Matter Phys. **5**, 57 (2014).

[4] J. Chaloupka, G. Jackeli, and G. Khaliullin, Kitaev-Heisenberg Model on a Honeycomb Lattice: Possible Exotic Phases in Iridium Oxides A_2IrO_3, Phys. Rev. Lett. **105**, 027204 (2010).

[5] Y. Singh, S. Manni, J. Reuther, T. Berlijn, R. Thomale, W. Ku, S. Trebst, and P. Gegenwart, Relevance of the Heisenberg-Kitaev Model for the Honeycomb Lattice Iridates A_2IrO_3, Phys. Rev. Lett. **108**, 127203 (2012).

[6] E. K.-H. Lee and Y. B. Kim, Theory of magnetic phase diagrams in hyperhoneycomb and harmonic-honeycomb iridates, Phys. Rev. B **91**, 064407 (2015).

[7] I. Kimchi, R. Coldea, and A. Vishwanath, Unified theory of spiral magnetism in the harmonic-honeycomb iridates α, β, and γli$_2$iro$_3$, Phys. Rev. B **91**, 245134 (2015).

[8] S. M. Winter, Y. Li, H. O. Jeschke, and R. Valentí, Challenges in design of Kitaev materials: Magnetic interactions from competing energy scales, Phys. Rev. B **93**, 214431 (2016).

[9] J. Chaloupka, G. Jackeli, and G. Khaliullin, Zigzag Magnetic Order in the Iridium Oxide Na$_2$IrO$_3$, Phys. Rev. Lett. **110**, 097204 (2013).

[10] R. D. Johnson, S. C. Williams, A. A. Haghighirad, J. Singleton, V. Zapf, P. Manuel, I. I. Mazin, Y. Li, H. O. Jeschke, R. Valentí, and R. Coldea, Monoclinic crystal structure of α-RuCl$_3$ and the zigzag antiferromagnetic ground state, Phys. Rev. B **92**, 235119 (2015).

[11] J. A. Sears, M. Songvilay, K. W. Plumb, J. P. Clancy, Y. Qiu, Y. Zhao, D. Parshall, and Y.-J. Kim, Magnetic order in α-RuCl$_3$: A honeycomb-lattice quantum magnet with strong spin-orbit coupling, Phys. Rev. B **91**, 144420 (2015).

[12] K. A. Modic, T. E. Smidt, I. Kimchi, N. P. Breznay, A. Biffin, S. Choi, R. D. Johnson, R. Coldea, P. Watkins-Curry, G. T. McCandless, J. Y. Chan, F. Gandara, Z. Islam, A. Vishwanath, A. Shekhter, R. D. McDonald, and J. G. Analytis, Realization of a three-dimensional spin-anisotropic harmonic honeycomb iridate, Nat. Commun. **5**, 4203 (2014).

[13] T. Takayama, A. Kato, R. Dinnebier, J. Nuss, H. Kono, L. S. I. Veiga, G. Fabbris, D. Haskel, and H. Takagi, Hyperhoneycomb Iridate β-Li$_2$IrO$_3$ as a Platform for Kitaev Magnetism, Phys. Rev. Lett. **114**, 077202 (2015).

[14] A. Biffin, R. D. Johnson, S. Choi, F. Freund, S. Manni, A. Bombardi, P. Manuel, P. Gegenwart, and R. Coldea, Unconventional magnetic order on the hyperhoneycomb Kitaev lattice in β-Li$_2$IrO$_3$: Full solution via magnetic resonant x-ray diffraction, Phys. Rev. B **90**, 205116 (2014).

[15] A. Biffin, R. D. Johnson, I. Kimchi, R. Morris, A. Bombardi, J. G. Analytis, A. Vishwanath, and R. Coldea, Noncoplanar and Counterrotating Incommensurate Magnetic Order Stabilized by Kitaev Interactions in γ-Li$_2$IrO$_3$, Phys. Rev. Lett. **113**, 197201 (2014).

[16] A. Ruiz, A. Frano, N. P. Breznay, Z. Islam, T. Helm, I. Oswald, J. Y. Chan, and J. G. Analytis, arXiv:1703.02531.

[17] J. P. Hannon, G. T. Trammell, M. Blume, and Doon Gibbs, X-ray Resonance Exchange Scattering, Phys. Rev. Lett. **61**, 1245 (1988).

[18] X. Liu, T. Berlijn, W.-G. Yin, W. Ku, A. Tsvelik, Y.-J. Kim, H. Gretarsson, Y. Singh, P. Gegenwart, and J. P. Hill, Long-range magnetic ordering in Na$_2$IrO$_3$, Phys. Rev. B **83**, 220403 (2011).

[19] Y. Feng, R. Jaramillo, J. Wang, Y. Ren, and T. F. Rosenbaum, Invited article: High-pressure techniques for condensed matter physics at low temperature, Rev. Sci. Instrum. **81**, 041301 (2010).

[20] W. B. Holzapfel, M. Hartwig, and W. Sievers, Equations of state for Cu, Ag, and Au for wide ranges in temperature and pressure up to 500 GPa and above, J. Phys. Chem. Ref. Data **30**, 515 (2001).

[21] H.-S. Kim, Y. B. Kim, and H.-Y. Kee, Revealing frustrated local moment model for pressurized hyperhoneycomb iridate: Paving the way toward a quantum spin liquid, Phys. Rev. B **94**, 245127 (2016).

[22] L. S. I. Veiga, M. Etter, K. Glaziryn, F. Sun, G. Fabbris, J. R. L. Mardegan, P. S. Malavi, Y. Deng, M. van Veenendaal, W. G. Yang, J. S. Schilling, T. Takayama, H. Takagi, and D. Haskel, Pressure-tuning of bond-directional exchange interactions and magnetic frustration in hyperhoneycomb iridate β-Li$_2$IrO$_3$, arXiv:1705.07059.

[23] D. Haskel, G. Fabbris, J. W. Kim, J. H. Kim, B. Kim, G. Cao, V. Struzhkin, P. P. Stavropoulos, H.-S. Kim, H.-Y. Kee, and S. Todadri (unpublished).

[24] Z. Zhao, S. Wang, T. F. Qi, Q. Zeng, S. Hirai, P. P. Kong, L. Li, C. Park, S. J. Yuan, C. Q. Jin, G. Cao, and W. L. Mao, Pressure induced second-order structural transition in Sr$_3$Ir$_2$O$_7$, J. Phys.: Condens. Matter **26**, 215402 (2014).

[25] A. Ruiz, N. P. Breznay, T. Helm, I. Oswald, J. Y. Chan, and J. G. Analytis (unpublished).

[26] K. A. Modic, B. J. Ramshaw, J. Betts, N. P. Breznay, J. G. Analytis, R. D. McDonald, and A. Shekhter, Robust spin correlations at high magnetic fields in the harmonic honeycomb iridates, Nat. Commun. (to be published), arXiv:1612.09410.

[27] D. Haskel, G. Fabbris, M. Zhernenkov, P. P. Kong, C. Q. Jin, G. Cao, and M. van Veenendaal, Pressure Tuning of the Spin-Orbit Coupled Ground State in Sr$_2$IrO$_4$, Phys. Rev. Lett. **109**, 027204 (2012). .

[28] M. A. Laguna-Marco, D. Haskel, N. Souza-Neto, J. C. Lang, V. V. Krishnamurthy, S. Chikara, G. Cao, and M. van Veenendaal, Orbital Magnetism and Spin-Orbit Effects in the Electronic Structure of BaIrO$_3$, Phys. Rev. Lett. **105**, 216407 (2010).

[29] J. P. Clancy, N. Chen, C. Y. Kim, W. F. Chen, K. W. Plumb, B. C. Jeon, T. W. Noh, and Y.-J. Kim, Spin-orbit coupling in iridium-based 5d compounds probed by x-ray absorption spectroscopy, Phys. Rev. B **86**, 195131 (2012).

[30] V. M. Katukuri, R. Yadav, L. Hozoi, S. Nishimoto, and J. van den Brink, The vicinity of hyper-honeycomb β-Li$_2$IrO$_3$ to a three-dimensional Kitaev spin liquid state, Sci. Rep. **6**, 29585 (2016).